ELSEVIER

Journal of Chromatography A, 726 (1996) 25–36

JOURNAL OF CHROMATOGRAPHY A

Intra-particle sorption rate and liquid chromatographic bandbroadening in porous polymer packings II. Slow sorption rate on a microparticle packing

Jingyi Li, Laurie M. Litwinson, Frederick F. Cantwell*

Department of Chemistry, University of Alberta, Edmonton, Alb., T6G 2G2, Canada

Received 7 June 1995; revised 14 September 1995; accepted 15 September 1995

Abstract

The rate of sorption of naphthalene from solution in methanol–water (85:15) onto 10-μm diameter particles of the macroporous poly(styrene–divinylbenzene) sorbent Hamilton PRP-1 is measured by the shallow-bed technique. The sorbent bed is 3 mm in diameter by about 0.3 mm high and contains only 1 mg of PRP-1. This bed is located in the slider of a very low hold-up volume valve. Linear velocity of naphthalene solution through the bed is high enough to exceed 400 bed volumes per second and the valve is capable of accurately providing flow times as short as 0.04 s. The curve of moles sorbed versus time is fit by an empirical tri-exponential rate equation. The parameters of this rate equation are used in a recently developed mathematical model to predict the plate heights and peak shapes of naphthalene peaks that would be expected to elute from a 15-cm long HPLC column of PRP-1 at various linear velocities, if intra-particle processes were the only source of bandbroadening.

The predicted peaks are close representations of the peaks that are experimentally observed to elute from such a PRP-1 column. This demonstrates that slow intra-particle processes are the major cause of bandbroadening of naphthalene on PRP-1.

Keywords: Band broadening; Sorption; Stationary phases, LC; Polymer packings, porous; Thermodynamic parameters; Kinetic studies; Naphthalene

1. Introduction

Porous poly(styrene–divinylbenzene) (PS–DVB) copolymers are reversed-phase liquid chromatographic packings which possess both advantages and disadvantages compared to silica-bound octadecylsilyl (ODS) packings. They exhibit greater chemical stability, especially at the extremes of pH, and they lack residual silanol groups [1–7]. However, they exhibit lower chromatographic efficiencies than ODS packings of comparable particle diameter. In fact, for some combinations of solute and mobile phase, the solute peak eluted from a PS–DVB column is extremely broad and tailing [8–11]. As solutes, polynuclear aromatic hydrocarbons are often particularly bad in this regard. Several possible reasons have been advanced to explain the sometimes very low efficiency observed on PS–DVB: (i) insufficient wetting of the pore surfaces which creates "stagnant zones" within the particles [10]; (ii) shrinking and swelling of the particles upon

*Corresponding author.

0021-9673/96/$15.00
SSDI 0021-9673(95)01017-3

solvent switching which causes channeling in the bed [12]; (iii) strong interaction of π-electrons in the polymer with the solute [9]; and (iv) slow diffusion of solute into the polymer matrix itself [13]. In the conventional view, it is the surface of the polymer matrix lining the meso- and macropores which acts as the sorbent (adsorbent) [2]. However, it has been cogently argued that the polymer matrix is also porous so that under some conditions, solvent and solute molecules can diffuse into it. The claim is that the polymer matrix has spaces (pores) between the polymer chains that are $\leq$20 Å in width [8,14]. Pores of $\leq$20 Å are called "micropores" [15]. Hence, in one view, diffusion into the polymer matrix can be interpreted as diffusion into micropores [8]. Of these four suggested reasons for low efficiency, (i), (iv) and probably (iii) would lead to a slow "intra-particle sorption rate". This could be slow diffusional mass transfer through the particle, a slow adsorption/desorption step or some combination of both.

The shallow-bed technique described in Part I [16] of this study is adapted to the measurement of sorption rates on a microparticle PS–DVB high-performance liquid chromatography (HPLC) column packing. Since sorption rates are generally faster on smaller particles, the achievement of "shallow-bed conditions" is much more challenging for microparticles than it is for large particles. The microparticle HPLC packing that is used is Hamilton PRP-1, a 10-μm diameter spherical packing that is used for reversed-phase HPLC [1–9,11,14,17–24]. In this study the intra-particle rate is measured for the sorption of naphthalene from methanol–water (85:15) solution onto a 0.30 mm long shallow-bed of PRP-1. A theoretical model was also developed and validated in Part I, by which the measured sorption-rate curve can be used to predict the contribution of intra-particle sorption rate to the shape of a peak eluted from an HPLC column [16]. The theoretical model is used in the present study to predict the intra-particle rate contribution to peak shape for naphthalene eluted from a 15×0.46 cm I.D. HPLC column of PRP-1 using methanol–water (85:15) as a mobile phase; and the predicted elution peak is compared to the experimentally-observed HPLC elution peak for naphthalene.

2. Experimental

2.1. Reagents and chemicals

Naphthalene (Coleman and Bell, Norwood, OH, USA) was recrystalized from methanol. Phloroglucinol (1,3,5-trihydroxybenzene, Fisher) was recrystallized from water. Methanol (Fisher) was reagent grade and was distilled before use. Water was distilled and deionized (Barnstead NANOpure System, Boston, MA, USA).

The solvent and eluent in both the sorption-rate experiments and the elution chromatography was always methanol–water (85:15, v/v). Before use in either type of experiment solutions and eluent were filtered through a 0.45-μm pore size Nylon 66 filter (Mandel Scientific Co.).

2.2. Sorbent

The macroporous PS–DVB sorbent PRP-1 (Lot No. 334, Hamilton Co., Reno, NV, USA) was used in the shallow-bed sorption-rate experiments. Characteristics of PRP-1 listed by the manufacturer include: spherical shape with 10-μm particle diameter (95% within the range 8–12 μm), specific pore volume of particles 0.79 cm^3/g, average pore diameter 75 Å, and specific surface area 415 m^2/g. Particle porosity, calculated from information supplied by the manufacturer, is 0.48 ml of pores per ml of a particle. Elution chromatography was performed on a 15.0× 0.46 cm I.D., factory-packed column of PRP-1 (part 79425-3145, Hamilton Co.) which, based on the manufacturer's information, has the following characteristics: bulk density 0.42 g/cm^3, inter-particle porosity 0.31 ml/ml, intra-particle porosity 0.33 ml/ml.

2.3. Sorption-rate apparatus

Fig. 1 is a diagram of the apparatus used for the shallow-bed sorption-rate experiments. P1 and P2 are constant-pressure pumps of a type previously described [25]. One contains 5×10^{-6} mol/l naphthalene in 85% methanol and the other contains 7×10^{-5} mol/l phloroglucinol in 85% methanol. Valve V1 is a six-port, stainless-steel rotary valve

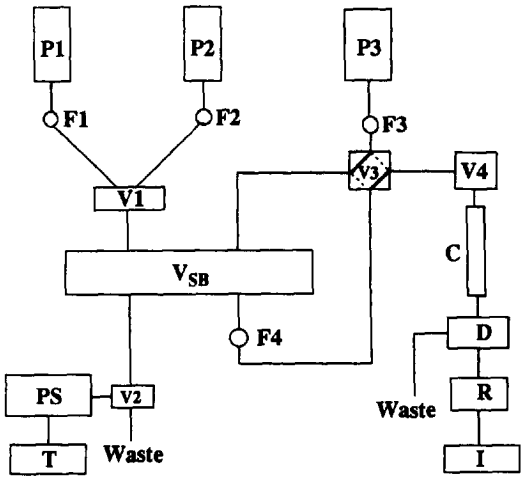

Fig. 1. Schematic diagram of the shallow-bed sorption rate apparatus. P1–P3: pumps; F1–F4: in-line filters; V1–V4: valves; C: μBondapak analytical HPLC column; D, R and I: detector, recorder and integrator. Flow through the left-hand side of the shallow-bed valve (V_{SB}) is turned on and off by valve V2, to which the position sensor (PS) and timer (T) are attached. See text for details.

(Model 204-01, Altex Corp.) which selects the solution to be pumped into the left-hand port of the shallow-bed valve V_{SB}. F1 and F2 are in-line filters (part no. XX4404700, Millipore Co.) containing 0.45-μm membrane filters (Durapore, part no. HVLP04700, Millipore). Valve V2 is a Cheminert 6-port rotary valve (part no. R6031V6, Laboratory Data Control) which is used as an on–off valve to determine whether or not the solution selected by V1 will flow through V_{SB}. Attached to V2 is a small infrared generator/detector, position sensor PS (ECG 3101 P312, Phillips, Dorval, Que., Canada) which is connected to a digital timer T (Model 5321B, Hewlett-Packard) set to display $\pm 10^{-4}$ second. The position sensor–timer device registers the time during which solution is flowing through the shallow bed.

Pump P3 is an HPLC pump (Model SP8000, Spectra-Physics Corp.) which pumps 85% methanol eluent at a constant flow-rate of 0.5 ml/min. The Cheminert four-way slider valve V3 (part no. CAV4031, LDC) either directs the flow of eluent directly to the injection valve V4 (part no. 7017, Rheodyne Corp.) as shown by the dashed lines, or first circulates the eluent through the right-hand side of V_{SB} as shown by the solid lines. C is a 15×0.46 cm HPLC column packed with μBondapak Phenyl sorbent (part No. 086680, Waters Corp.). F3 and F4 are low dead-volume, in-line filters (part 7315, Rheodyne, Berkeley, CA, USA) containing 2-μm stainless steel filter elements.

The shallow-bed slider valve V_{SB} is the heart of the system. It is shown in Fig. 2, which is not drawn to scale. The stainless-steel valve body is composed of two parallel outer plates with four tension adjustment screws, two parallel inner plates against which the tension screws exert their force, and two end plates. The outer plates are bolted together and the end plates are bolted to them. Underlying the inner steel plates are Teflon face plates. A piece of Teflon tape is placed between the steel and Teflon plates to insure a good seal. The slider is held between the Teflon face plates. The slider is a 2 mm thick×13 mm wide×113 mm long flat piece of stainless steel, the center of which is cut out and holds a 2.2 mm high×9 mm wide×73 mm long piece of Kel-F with two 3-mm diameter holes drilled through it. The Teflon face plates contact only this Kel-F insert. The hole on the right is empty and the hole on the left contains a stainless-steel screen at the bottom. This screen is 0.076 mm thick and has 2-μm pores. It serves as the support for the shallow-bed which

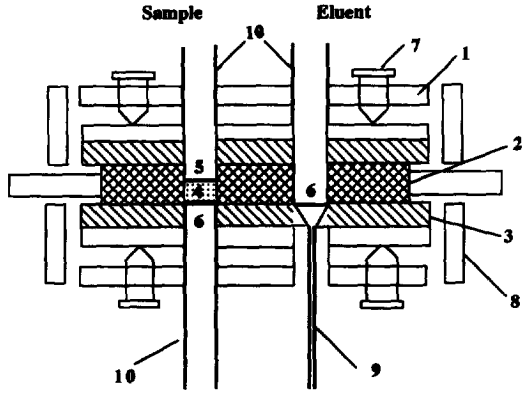

Fig. 2. Schematic diagram of the shallow-bed slider valve V_{SB}, in Fig. 1. Not to scale. 1,8: SS body plates; 2: Kel-F insert in slider; 3: Teflon face plate; 4: bed of PRP-1; 5: porous Teflon disks; 6: SS screens; 7: tension-adjustment screws; 9: 0.05-mm I.D. SS tube; 10: 3-mm I.D. SS tubes.

contains about 1 mg of PRP-1, accurately weighed, spread uniformly over the screen to a depth of about 0.3 mm. On top of the PRP-1 are two 3-mm diameter disks of Zitex porous Teflon membrane. The lower one is 0.2 mm thick and has 10–20 μm pores (part H662-123, Chemplast Corp. Wayne, NJ, USA) and the upper one is 0.64 mm thick and has 30–60 μm pores (part K1064-222). The whole valve is bolted to a back plate (not shown) and the slider is moved left and right by a pair of metal levers which are also attached to the back plate.

Flow into the left and right holes of the slider is accommodated by 3-mm I.D. stainless steel hypodermic needle tubing that passes through holes drilled through the outer and inner steel plates, and is silver soldered to the latter; and by 3-mm I.D. holes in the Teflon face plate. Flow out of the left hole is accommodated in the same way. The inlet and outlet tubes on the left have the same 3-mm diameter as the bed of PRP-1 in order to insure uniform flow, which prevents disturbances to the bed and facilitates achievement of shallow-bed conditions during the sorption step. Flow out of the right-hand hole occurs via 1/16″ O.D.×0.002″ I.D. (1.6 mm×0.05 mm) stainless-steel tubing soldered in a hole through the inner stainless-steel plate. The small I.D. is important to minimize bandbroadening during the elution step. A constant temperature of 25.0±0.2°C was achieved by immersing P1, P2, F1, F2, V_{SB}, and all tubing in a thermostatted water bath.

Solute eluted from the shallow bed when it is in the right-hand position is chromatographed on column C and quantified by means of a UV-absorbance detector D (Spectroflow 757, Kratos Analytical Instruments), a Recordall recorder R (Fisher) and a digital integrator I (HP3390A, Hewlett-Packard). The detector, set at 276 nm, was calibrated by injecting a series of standards into column C by means of valve V4 fitted with a 20-μl sample loop.

2.4. Sorption-rate measurement

With the bed of PRP-1 in the right-hand position in V_{SB}, 85% methanol is pumped through it from P3 during the pre-equilibration step. Then V3 is switched to bypass the bed, and the slider in V_{SB} is moved to the left. At this time V2 is in the off position so that sample solution does not flow through the bed of PRP-1.

Valve V2 is switched to the on position, which starts both the timer and the flow of sample solution containing 5×10^{-6} moles naphthalene per liter. This is the sorption step. When the desired exposure time of PRP-1 to the flowing solution has elapsed, valve V2 is switched to the off position which immediately stops the flow and the timer. In this apparatus the minimum sorption time is 0.04 s, which is determined by the minimum time it takes to rotate V2 through the on to an off position.

The slider in V_{SB} is next moved to the right-hand position and V3 is switched to cause the 85% methanol from P3 to flow through the bed in order to elute naphthalene from the PRP-1, through column C to the detector. This is the desorption step.

The moles of naphthalene sorbed per gram of PRP-1 (C_S) at a given time is calculated via Eq. 14 in Part I [16]. The hold-up volume, V_{HU}, is measured by equilibrating the shallow bed with a 7×10^{-5} mol/l solution of phloroglucinol in 85% methanol, eluting and measuring the amount of phloroglucinol in the bed. Phloroglucinol is not adsorbed by PRP-1 but it does enter all void spaces, including pore spaces in the PRP-1 particles. For a bed containing 1.12×10^{-3} g of PRP-1 V_{HU} was 9.2±0.9 μl and V_{pore} was 0.86±0.06 μl.

2.5. Elution chromatography

Chromatography of naphthalene on the 15-cm long column of PRP-1 was performed using only pump P3, injection valve V4, detector D and recorder R from the apparatus depicted in Fig. 1. Twenty-microliter volumes of 3×10^{-5} mol/l of naphthalene in 85% methanol were injected into the 85% methanol eluent. The concentration of naphthalene in the injected solution was made very low in order to insure that it would be in the linear part of the naphthalene sorption isotherm. The eluent flow-rate was varied from 0.5 to 2 ml/min in these experiments. Replicate injections were made at each flow-rate. The elution peaks on the strip chart recorder were manually digitized at 12 or 24 s intervals of time. The extra-column contribution to the retention volume due to injector (20 μl), detector (14 μl) and connecting tubing (0.7 μl) is small and is neglected

in calculations associated with the observed and predicted elution peaks of naphthalene.

The retention time of an unretained component, t_M, was measured at each flow-rate by making replicate 20-μl injections of a 5×10^{-4} mol/l solution of phloroglucinol in 85% methanol. The first statistical moment of the symmetrical phloroglucinol peak was used to calculate the retention time t_M, the column void volume V_M, and the linear velocity of the mobile phase U_0.

2.6. Sorption isotherm measurement

The sorption isotherm of naphthalene on PRP-1 was measured in the apparatus shown in Fig. 1, employing the "column-equilibration technique" [26]. Solutions containing various concentrations of naphthalene in 85% methanol were pumped through a 1.09×10^{-3} g bed of PRP-1 for 60 s, by which time naphthalene has come very close to sorption equilibrium, as will be shown below [16]. The steps in the procedure and the calculations are the same as those listed above for measuring the sorption-rate curve by the shallow-bed method.

3. Results and discussion

Both the experimental concept and the theoretical model that are employed in this study have been described and validated in Part I of this series [16]. In order to measure sorption rates on PRP-1 it was necessary to construct and characterize a new apparatus. The characteristics of the apparatus, the sorption-rate curve measured with it, and the important role played by intra-particle sorption rate in the chromatographic bandbroadening of naphthalene on PRP-1 are discussed below.

3.1. Shallow-bed conditions

The critical difference between the previous study [16], in which XAD-2 particles of 0.36-mm diameter were used, and the present study, in which PRP-1 particles of 0.010-mm diameter are used, is the very much faster sorption rate encountered in the present study. In the sorption-rate experiment it is necessary to achieve shallow-bed (infinite bath) kinetic conditions, in which all particles in the bed, at all times, are bathed in a solution whose solute concentration is the same as that at the inlet to the bed; and it is also necessary to eliminate film diffusion as a contributor to sorption rate. In addition, data points have to be collected at much shorter times than was true for the XAD-2 study.

As the interstitial linear velocity of solution through the bed (U_{inter}, cm/s) is increased, conditions in the bed approach more closely those of a shallow bed and the thickness of the Nernst diffusion film around the particles decreases. At sufficiently high U_{inter} the desired conditions are met and the rate of sorption becomes independent of the linear velocity of solution. This serves as the basis of an experimental test [16]. Since film diffusion makes its greatest contribution early in the experiment, only the initial rates need to be measured for this test. During the initial 0.05 s, the sorption-rate curves are approximated to be linear. Their slopes are presented as a function of both flow-rate and U_{inter} in Table 1. It can be seen that for $U_{inter} \gtrsim 16$ cm/s, sorption rate is independent of U_{inter}; meaning that the bed of PRP-1 acts as a shallow bed and the observed sorption rate is equal to the intra-particle sorption rate. In subsequent measurements of the sorption-rate curve U_{inter} was always greater than 16 cm/s. For this bed a linear velocity of 16 cm/s corresponds to the passage of over 400 bed volumes of solution per second.

3.2. Linear sorption isotherm

Shown in Fig. 3 is a plot of moles of naphthalene sorbed per gram of PRP-1 at equilibrium versus concentration of naphthalene in methanol–water (85:15). The solid line in Fig. 3 is a fit of the Langmuir equation to the data points. The isotherm is linear up to a solution concentration of approximately 4×10^{-5} mol/l (dashed line). The slope of $(3.9\pm0.1)\times10^{-2}$ l/g, is equal to the mass–volume distribution coefficient for naphthalene. Since sorption-rate experiments were performed at a solution concentration of 5×10^{-6} mol/l, they clearly were performed in the linear part of the isotherm.

Table 1
Initial sorption rates over the first 0.05 second on the 1.12-mg bed of PRP-1 as a function of flow-rate and interstitial linear velocity of solution through the bed in order to verify shallow-bed conditions

F (ml/min)	U^{a}_{inter} (cm/s)	No. bed volume per s[b]	Initial rate[c] (mol/g/s)
16.6	12.6	335	2.9×10^{-10}
21.6	16.4	435	6.3×10^{-10}
25.1	19.1	506	7.4×10^{-10}
27.1	20.6	546	6.9×10^{-10}
31.6	24.0	637	6.1×10^{-10}
37.5	28.5	756	6.9×10^{-10}

[a] U_{inter} is calculated via Eq. 16 in Ref. [16], using r=0.15 cm bed radius, and ε_{inter}=0.31 from Ref. [17].
[b] Interstitial (i.e. inter-particle) bed volume is 0.83 μl for this 1.12 mg shallow bed of PRP-1.
[c] Absolute initial rates cannot be compared directly with those in Table 1 of Ref. [16] because solute concentrations in solution and distribution coefficients differ.

3.3. Sorption-rate curve

Shown in Fig. 4 is a typical sorption-rate curve for naphthalene on the shallow bed of PRP-1. The points are experimental, with the first one measured at 0.040 s and the last one measured at 69.3 s. The vertical axis variable F is the fraction of the equilibrium moles of naphthalene that has been sorbed at any time. Examination of the data points shows that about 0.5 (i.e. 50%) of the naphthalene is sorbed within 0.2 s and about 0.9 is sorbed within 1.0 s. After about 2 s the rate of sorption is very much slower, but finite.

The solid line through the data points results from a tri-exponential fit of the data. The equation of this line has the form [16]:

$$F = 1 - \frac{n_1}{n_0}\exp(-k_1 t) - \frac{n_2}{n_0}\exp(-k_2 t) - \frac{n_3}{n_0}\exp(-k_3 t) \quad (1)$$

In this expression n_1 through n_3 are the moles of solute sorbed per gram at equilibrium whose sorption rate can be described by the first-order rate constants k_1 through k_3, respectively. The total moles sorbed per gram at equilibrium is n_0 where:

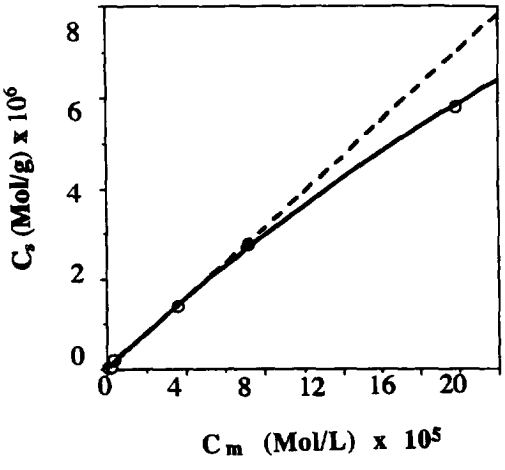

Fig. 3. Equilibrium sorption isotherm of naphthalene between PRP-1 and 85% methanol. Solid line is Langmuir fit. Dashed line extrapolates linear region.

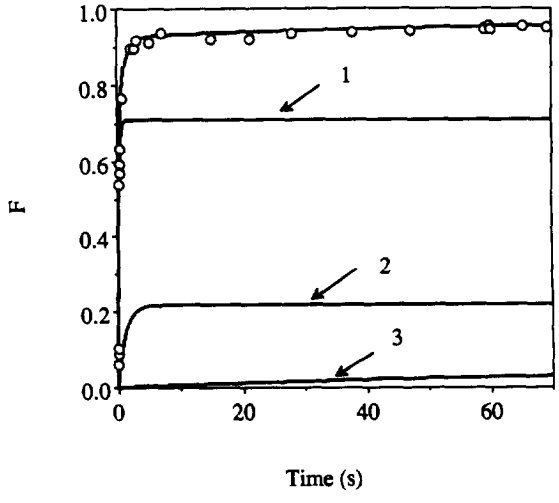

Fig. 4. Sorption-rate curve of naphthalene on PRP-1 from 85% methanol. Points are experimental. Un-numbered line is tri-exponential fit (Eq. 1). At 60 s, sorption is about 95% of the way to equilibrium. Numbered curves represent contributions of the j=1, 2 and 3 terms, respectively, in Eq. 1.

$$n_0 = n_1 + n_2 + n_3 \quad (2)$$

As discussed previously [16], the use of a multi-exponential equation to represent the data is purely empirical and is based on no theoretical model of physically real processes occurring within the PRP-1 particle. A tri-exponential equation was employed, rather than, for example, a mono-, bi- or tetra-exponential equation, because a tri-exponential is the multi-exponential equation with the smallest number of exponential terms that accurately represents this particular set of experimental data over the whole curve. It is essential to realize that the model which is employed requires a sum of exponential terms rather than any other emperial equation, and that it is not compromised by the fact that there may be strong correlation among some of the n_j and k_j parameters [16]. Eq. 1 was fit to the data points by a non-linear least-squares program in the software package MatLab [27]. The six parameters, k_1–k_3 and n_1–n_3, which describe the solid line in Fig. 4, are presented in the second column of Table 2, labeled run 1. The three numbered curves in Fig. 4 correspond, respectively, to the first, second and third exponential terms in Eq. 2 for run 1, considered individually [16].

The sorption-rate experiment was repeated four additional times. The n_j and k_j constants obtained from the tri-exponential fitting of the sorption-rate data in these experiments appear in the vertical columns labeled run 2, 3, 4, and 5 in Table 2. The linear velocities used in all five of the sorption-rate experiments are shown in the first row of Table 2. All of them are high enough to achieve both shallow-bed conditions and intra-particle sorption-rate control. When intercomparing the n_j and k_j values among the five replicate runs in Table 2 it is important to bear in mind two facts. First, these constants have no physical reality, but are merely empirical curve fitting parameters. Second, the six constants in Eq. 1 are not fully independent of one another, so that for a given set of experimental data (e.g. run 1) there may be several different combinations of the six constants that yield nearly equally good fits to the data. This situation creates no problem in using Eq. 1, either in representing the sorption-rate data or in predicting elution chromatographic peak shapes. As previously discussed [16], the ambiguities in the values of n_3 and k_3 can be eliminated by accepting the set of n_3 and k_3 which simultaneously satisfies the following two criteria: (i) minimum value of the χ^2 fitting parameter and, (ii) smallest value of n_3. The overall agreement between the tri-exponential equation and the sorption-rate data is indicated for each run by χ^2 at the bottom of each column in Table 4.

3.4. Predicted vs. observed elution peaks

According to the formalistic concept that has been elaborated in Ref. [16], a chromatographic column of

Table 2
Constants for the tri-exponential equation (Eq. 1) which describe the five replicate sorption-rate curves for naphthalene on a shallow bed of PRP-1

Parameter	Run[a]				
	1[b]	2	3	4	5[c]
U_{inter}(cm/s)	19.1	24.0	20.6	17.6	20.2
k_1 (s^{-1})	4.23	19.6	11.1	3.95	6.64
k_2 (s^{-1})	0.85_3	2.70	1.37	0.60_8	0.203
k_3 (s^{-1})	0.012_0	0.14_9	0.030_9	0.024_4	4.94
n_1 (mol/g)	7.8×10^{-8}	2.5×10^{-8}	5.7×10^{-8}	6.7×10^{-8}	1.1×10^{-7}
n_2 (mol/g)	2.4×10^{-8}	7.8×10^{-8}	4.9×10^{-8}	1.4×10^{-8}	3.4×10^{-8}
n_3 (mol/g)	5.6×10^{-9}	9.9×10^{-9}	6.7×10^{-9}	6.8×10^{-9}	3.1×10^{-15}
n_0 (mol/g)	1.1×10^{-7}	1.1×10^{-7}	1.1×10^{-7}	8.9×10^{-8}	1.4×10^{-7}
χ^{2d}	6.4×10^{-9}	6.5×10^{-9}	5.4×10^{-9}	8.1×10^{-9}	1.4×10^{-8}

[a] Shallow bed contained 1.12×10^{-3} g of PRP-1 in runs 1–4, and 9.4×10^{-4} g in run 5.
[b] Sorption-rate curve for run 1 is shown in Fig. 4.
[c] For run 5, a bi-exponential equation gives as good a fit as a tri-exponential equation.
[d] χ^2 for nonlinear fit by Eq. 1.

length L packed with PRP-1 is assumed to possess three different types of hypothetical sorption sites whose fractional amounts are n_1/n_0, n_2/n_0 and n_3/n_0, based on the tri-exponential fitting of the sorption-rate data by Eq. 1 (Fig. 4; Table 2). The chromatographic column is then represented by three hypothetical columns placed in series, each of which contains only one of the three types of sites. Each of these hypothetical columns therefore corresponds to one of the terms in Eq. 1, having the form $(n_j/n_0)\exp(-k_j t)$. Also, each of the three hypothetical columns has the same length (L), linear velocity of mobile phase (U_0), retention time of an unretained component (t_M), retention volume of an unretained component (V_M), and weight of PRP-1 sorbent (W_{col}), as the real chromatographic column has.

In order to predict the shape of the elution peak for naphthalene which would arise from bandbroadening due exclusively to intra-particle sorption rate, it is necessary to know the values of n_1 through n_3 and k_1 through k_3 obtained from Eq. 1. It is necessary also to know the value of the capacity factor (k') for naphthalene on the chromatographic column in question, and to know the retention time of an unretained component. In this study the chromatographic column of PRP-1 was 15 cm long and the mobile phase was methanol–water (85:15). Four different linear velocities of mobile phase were employed to obtain elution chromatograms. For the chromatogram at each U_0 the value of t_M was taken as the first statistical moment (i.e. center-of-gravity) of the unretained component phloroglucinol [28,29]. Values of t_M measured at the four linear velocities are presented in the second column of Table 3. The corresponding linear velocities were calculated from the expression:

$$U_0 = \frac{L}{t_M} \tag{3}$$

The values of k' for naphthalene in the third column of Table 3 were calculated from the expression:

$$k' = \frac{t_R - t_M}{t_M} \tag{4}$$

where t_R is the first statistical moment of the experimentally observed elution peak for naphthalene (to be discussed below). As expected [28,29], k' is independent of U_0.

The steps involved in predicting elution peak shape from the sorption-rate curve have been exemplified in Fig. 2 of Part I [16]. The last step in that operation is a convolution of the peak with the peak due to an unretained component. As was true for the system studied in Part I, the variance of the unretained-component peak in the present study (e.g., 6.3 s^2 at U_0=0.30 cm/s) is so small compared to the variance of the sample (naphthalene) peak (e.g., 2.40×10^4 s^2 at U_0=0.30 cm/s) that this final convolution step increases the center-of-gravity of the naphthalene peak by t_M, but makes a negligible increase in its variance.

The experimentally measured first-order rate constants (k_j) for reversible sorption of naphthalene on the hypothetical column j=1, 2 and 3 are given in Table 2, along with corresponding n_j and n_0 values. Typical values of the adsorption (i.e., forward) first-order rate constants $k_{a,j}$ and of the desorption (i.e., reverse) first-order rate constants $k_{d,j}$ for naphthalene on hypothetical columns j, calculated using n_j and k_j values obtained from the sorption-rate curve shown in Fig. 4 (i.e. run 1), are: $k_{a,1}$=4.03 s^{-1}, $k_{a,2}$=0.736 s^{-1}, $k_{a,3}$=0.0072 s^{-1}, $k_{d,1}$=0.196 s^{-1}, $k_{d,2}$=0.117 s^{-1} and $k_{d,3}$=0.0048 s^{-1}. In the last column of Table 3 are given the values of the term $\exp(-k_{a,3}t_M)$ which is the fraction of naphthalene not sorbed on hypothetical column 3. At higher U_0 the fraction not sorbed increases. For hypothetical columns 1 and 2 the fraction of naphthalene not sorbed is negligible (i.e. $<10^{-10}$) at all four U_0 employed.

The manner in which a predicted elution peak may be compared with an observed elution peak [16] can be exemplified using the peak which is predicted to

Table 3
Parameters obtained from the observed elution chromatograms and fraction of naphthalene not sorbed on hypothetical column 3

U_0 (cm/s)	t_M^a (s)	k'^b	$\exp(-k_{a,3}t_M)$
0.10	153±2	28.9±0.4	0.333
0.20	77.3±0.5	28.0±0.3	0.574
0.30	50.5±0.5	28.0±0.3	0.696
0.40	37.9±0.7	29.0±0.5	0.762

[a] t_M is from observed elution chromatogram of phloroglucinol.
[b] k' is from observed elution chromatogram of naphthalene.

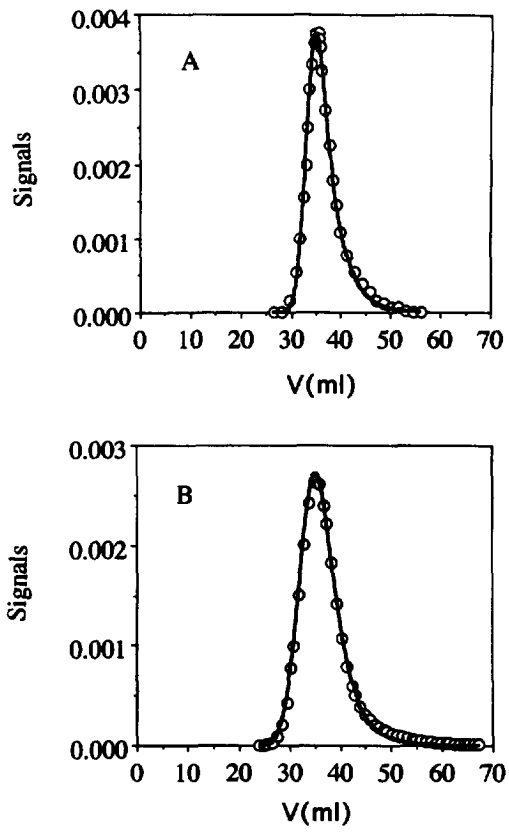

Fig. 5. Typical elution peak (points) and EMG-fit (line) that are observed (A) and predicted (B) for elution of naphthalene from a 15-cm long HPLC column of PRP-1 at U_0=0.30 cm/s. Predicted peak in panel B is calculated from sorption-rate run 1.

elute from a 15-cm long column of PRP-1 at U_0= 0.30 cm/s. A typical observed elution peak, obtained under these conditions, is presented as the data points in Fig. 5A. The corresponding predicted peak is presented as the points in Fig. 5B. The first step in comparing these two peaks is to fit the points in each using the equation of an exponentially-modified Gaussian (EMG) peak. The solid lines in Fig. 5A and 5B are the EMG-peaks. Next, the following figures of merit are obtained for the EMG peaks: The first statistical moment (center-of-gravity) of the overall peak (V_R), which is the sum of the first moments of the Gaussian part (V_G) and the exponential part (V_{exp}); the second central moment (variance) of the overall peak (σ^2), which is the sum of the variances of the Gaussian part (σ_G^2) and the exponential part (σ_{exp}^2); the plate height of the column, which is given by the expression:

$$H = L\frac{\sigma^2}{V_R^2} = L\frac{\sigma_G^2 + \sigma_{exp}^2}{(V_R + V_{exp})^2} \quad (5)$$

and the asymmetry factor (A.F.), which is measured graphically at 0.1 of the peak height [30]. The predicted and observed peaks can then be compared in terms of these figures of merit.

These comparisons are summarized in Table 4 at four mobile phase linear velocities: 0.10, 0.20, 0.30, and 0.40 cm/s. Five replicate sorption-rate curves were measured, each of which yielded a unique set

Table 4
Chromatographic figures of merit for observed (OBS) and predicted (PRE) elution peaks of naphthalene on a 15-cm column of PRP-1. Averages and standard deviations

U_0 (cm/s)	Peak	V_R (ml)	V_G (ml)	V_{exp} (ml)	σ^2 (ml^2)	σ_G^2 (ml^2)	σ_{exp}^2 (ml^2)	H (mm)	A.F.
0.10	PRE	37.4±0.5	35.2±0.5	2.0±0.7	7.3±2.1	3.8±0.8	4.3±2.9	0.8±0.2	1.4±0.3
	OBS	38.8±0.8	36.0±0.9	2.7±0.1	9.1±0.2	1.6±0.4	7.5±0.1	0.9±0.1	2.2±0.2
0.20	PRE	37.5±0.5	34.6±0.6	2.7±0.7	14±3	6.5±1.6	7.6±3.3	1.5±0.2	1.4±0.2
	OBS	37.8±0.5	35.1±0.7	2.7±0.2	9.5±0.9	2.1±0.2	7.4±1.1	1.0±0.1	1.9±0.0
0.30	PRE	36.7±0.3	33.3±0.7	3.1±0.7	19±3	8.7±2.1	10±4	2.2±0.3	1.5±0.2
	OBS	38.1±2.1	36.3±2.5	3.5±0.4	15±3	2.5±0.2	13±3	1.6±0.2	2.2±0.1
0.40	PRE	37.3±0.6	33.1±0.9	3.6±0.7	24±4	10±2	14±5	2.6±0.4	1.4±0.1
	OBS	37.0±1.0	33.2±1.1	3.8±0.6	17±4	2.2±0.1	15±5	1.9±0.5	2.3±0.3

of k_j and n_j constants (Table 2) from which an elution peak was predicted for a given linear velocity of mobile phase. Thus, for each of the four linear velocities, five replicate predicted elution peaks were calculated and all five were fit with an EMG function from which figure-of-merit parameters were obtained. Averages and standard deviations for these parameters are presented in rows 1, 3, 5, and 7 in Table 4 for the predicted peaks. In separate experiments replicate elution chromatograms of naphthalene were measured at the four linear velocities. In rows 2, 4, 6, and 8, of Table 4 are presented the averages and standard deviations of the figure-of-merit parameters obtained for these observed elution peaks.

In order to provide visual comparison of observed and predicted peaks, a typical observed peak is shown as data points in Fig. 6 for each linear velocity, along with a corresponding typical predicted peak based on the set of n_j and k_j from run 1, which is shown as a solid line. These observed points and predicted lines are not the EMG peaks. The points in Fig. 6C are the same as the points in Fig. 5A, and the solid line in Fig. 6C is the same as the points in Fig. 5B.

Visual comparison of the typical predicted and observed peaks in Fig. 6 suggests that the former are good approximations of the latter at all four linear velocities of mobile phase. Quantitative comparison, made by applying the t-test at each linear velocity of mobile phase, reveals that at the 95% confidence level the predicted and observed members of the pairs of values for V_R, V_G, V_{exp}, σ^2, H and A.F. cannot statistically be distinguished from one another. This is even more true for the square root of H, which has been suggested as a criterion of comparison [16]. The standard deviations for the observed-peak parameters are comparable in magnitude to those for the predicted-peak parameters. The reason for this is associated with the inherent uncertainties in quantitatively describing asymmetric peaks which exhibit kinetic tailing [16].

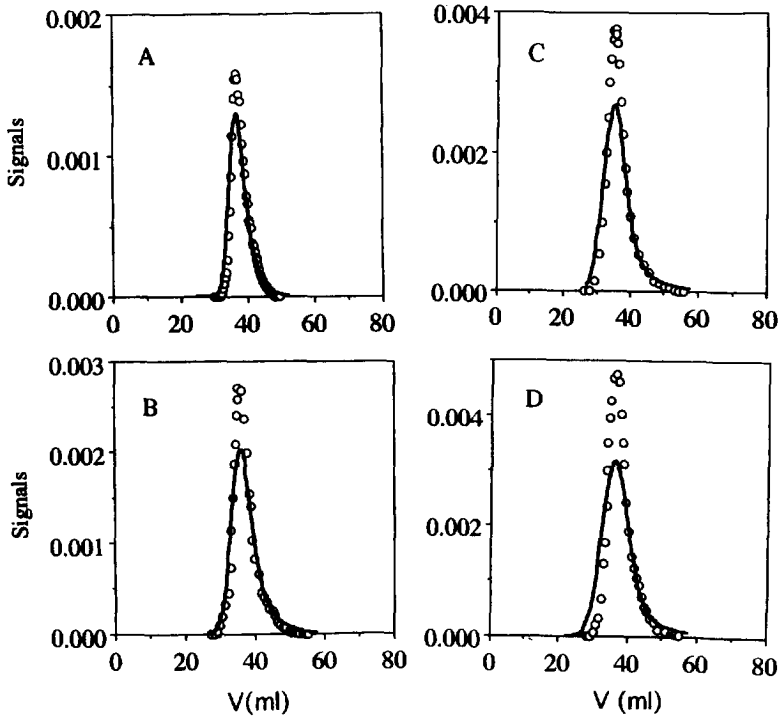

Fig. 6. Comparison of typical observed (points) and predicted (lines) peaks for elution of naphthalene from a 15-cm long HPLC column of PRP-1 at U_0=0.10 cm/s (A), 0.20 cm/s (B), 0.30 cm/s (C), and 0.40 cm/s (D). These are not the EMG-fit curves. Predicted peaks are calculated from sorption-rate run 1.

It is necessary, in practice, to represent chromatographic peaks by some analytical function, such as the EMG, in order to compute statistical moments that are free of the extreme ambiguities which would otherwise arise from baseline-setting errors [16]. However, such an arbitrary division of a chromatographic peak into a Gaussian and an exponential component is quite sensitive to small differences in peak shape, so that the relative contributions of σ_G^2 and σ_{exp}^2 to σ^2 may vary considerably between observed and predicted peaks while σ^2 itself exhibits close agreement between these peaks. This is seen in Table 4.

4. Conclusions

The peaks predicted above take into account only the bandbroadening which arises from intra-particle sorption rate (i.e. associated with only the H_S and H_{SM} terms in chromatographic rate theory). The close agreement between predicted and observed peaks therefore demonstrates that slow intra-particle sorption is, by far, the major bandbroadening process for naphthalene on the PS–DVB sorbent PRP-1. This is a highly informative conclusion of this study, because it constitutes direct evidence to support earlier suggestions that slow intra-particle processes are responsible for low chromatographic efficiencies and tailing peaks [8–11,13]. The extreme slowness of these processes for naphthalene on PRP-1 can be appreciated by noting that a plate height of 1 to 2 mm, as found in this study, corresponds to a reduced plate height of 100 to 200, which is very large [31].

The nature of the physical process within the PRP-1 particles which is responsible for the slow sorption rate of aromatic compounds has been investigated in detail in this laboratory. The results, which strongly implicate diffusion of solute into the polymer matrix as the slow process, are the subject of Part III of this series [32].

Acknowledgments

The Hamilton Co. kindly donated both the PRP-1 sorbent and the factory-packed HPLC column. The Chemistry Department Machine Shop at the University of Alberta fabricated the shallow-bed apparatus. Kinetic run 5 was performed by Barbara Ells in this laboratory. This work was supported by the Natural Sciences and Engineering Research Council of Canada and the University of Alberta.

References

[1] D.P. Lee, J. Chromatogr. Sci., 20 (1982) 203.
[2] D.J. Pietrzyk, in P.R. Brown and R.A. Hartwick (Editors), High Performance Liquid Chromatography (Chem. Anal.), Vol. 98, Wiley, New York, 1989, Chapter 10.
[3] A.M. Krstulovic and P.R. Brown, in Reversed-Phase High Performance Liquid Chromatography: Theory and Biomedical Applications, Wiley, New York, 1982, pp. 85–88.
[4] R.M. Smith, K.C. Madahar and W.G. Salt, Chromatographia, 19 (1985) 411.
[5] S.E. Tetl, D.J. Cutler and K.F. Brown, J. Chromatogr., 344 (1985) 241.
[6] M.J. Cope and I.E. Davidson, Analyst, 112 (1987) 417.
[7] S. Coppi and A. Betti, J. Chromatogr., 472 (1989) 406.
[8] F. Nevejans and M. Verzele, J. Chromatogr., 406 (1987) 325.
[9] J.R. Benson and D.J. Woo, J. Chromatogr. Sci., 22 (1984) 386.
[10] R.M. Smith and D.R. Garside, J. Chromatogr., 407 (1987) 19.
[11] L.D. Bowers and S. Pedigo, J. Chromatogr., 371 (1986) 243.
[12] W.R. Melander and C. Horvath, in C. Horvath (Editor), High Performance Liquid Chromatography: Advances and Perspectives, Vol. 2, Academic Press, New York, 1980, Chapter 3.
[13] D. Liru, H. Xizhang, W. Quhui, M. Qingcheng, L. Yuliang and Z. Youliang, Scientia Sinica (Series B), 25 (1982) 905.
[14] F. Nevejans and M. Verzele, Chromatographia, 20 (1985) 173.
[15] IUPAC, Manual of Symbols and Terminology, Appendix 2, Part I, Pure Appl. Chem., 31 (1972) 578.
[16] D. Gowanlock, R. Bailey and F.F. Cantwell, J. Chromatogr. A, 726 (1996) 1.
[17] D.P. Lee, J. Chromatogr., 443 (1988) 143.
[18] D.P. Lee and J.H. Kindsvater, Anal. Chem., 52 (1980) 2425.
[19] C.D. Raghuvuran, J. Liq. Chromatogr., 8 (1985) 537.
[20] R.M. Smith, J. Chromatogr., 29 (1984) 372.
[21] R.L. Smith, Z. Iskanderani and D.J. Pietrzyk, J. Liq. Chromatogr., 7 (1984) 1935.
[22] M. Verzele and Y.B. Yang, J. Chromatogr., 387 (1987) 197.
[23] L.L. Lloyd, J. Chromatogr., 554 (1991) 201.
[24] F.P. Warner and L.L. Lloyd, J. Chromatogr., 512 (1990) 365.
[25] L. Fossey and F.F. Cantwell, Anal. Chem., 54 (1982) 1693.
[26] S. May, R.A. Hux and F.F. Cantwell, Anal. Chem., 54 (1982) 1279.
[27] MATLAB™, The Mathworks, Inc., Natick, MA.
[28] J. Villermaux, J. Chromatogr., 406 (1987) 11.
[29] J. Villermaux, J. Chromatogr. Sci., 12 (1974) 822.

[30] J.C. Giddings, Dynamics of Chromatography, Dekker, New York, 1965, Chapters 2 and 6.
[31] J.C. Giddings and H. Eyring, J. Phys. Chem., 59 (1955) 416.
[32] J.C. Giddings, Anal. Chem., 35 (1963) 1999.
[33] J.J. Kirkland, W.W. Yau, H.J. Stoklosa and D.H. Dilks, Jr., J. Chromatogr. Sci., 15 (1977) 303.
[34] J.H. Knox, J. Chromatogr. Sci., 15 (1977) 352.
[35] J. Li and F.F. Cantwell, J. Chromatogr. A, 726 (1996) 37.